Powder Technology 435 (2024) 119348

Contents lists available at ScienceDirect

Powder Technology

journal homepage: www.journals.elsevier.com/powder-technology

Control of segregation by non-uniform aeration in a fluidized bed spray granulator

A. Atxutegi [a,*], M. Atzori [b], J. Bettien [a], T. Lichtenegger [b], S. Puttinger [b], S. Pirker [b], S. Heinrich [a]

[a] Institute of Solids Process Engineering and Particle Technology, Hamburg University of Technology (TUHH), Denickestrasse 15, 21073 Hamburg, Germany
[b] Department of Particulate Flow Modelling, Johannes Kepler University, Altenberger Str. 69, 4040 Linz, Austria

HIGHLIGHTS

- CFD-DEM simulations were run in a new actuated distributor plate.
- The aeration of the system was controlled and experimentally checked.
- A clear change in fluidization topology was immediately observed.
- Experimental confirmation of the change in particle segregation was found.
- Simulations allowed for a time dependent segregation analysis of the bed.

GRAPHICAL ABSTRACT

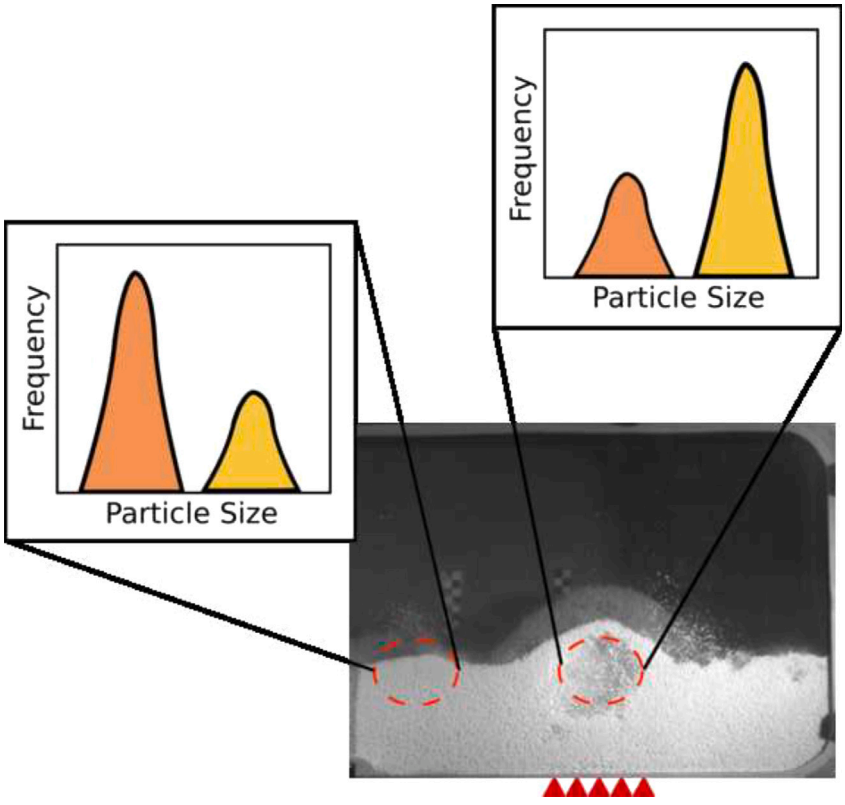

ARTICLE INFO

Keywords:
Fluidized spray granulation
CFD-DEM
Particle segregation

ABSTRACT

Controlling and influencing the rate of particle growth in spray granulators is key for consistent product quality and size, while reducing energy consumption and product re-circulation. To this end, we have implemented a new control device to actively change the fluidization topology of fluidized spray granulators and to influence

* Corresponding author.
E-mail address: aitor.achutegui@tuhh.de (A. Atxutegi).

https://doi.org/10.1016/j.powtec.2023.119348
Received 7 July 2023; Received in revised form 2 December 2023; Accepted 28 December 2023
Available online 18 January 2024

Granulation control

the local particle segregation in the areas affected by the granulation, selectively growing fine particle fractions at will. Simulations using computational fluid dynamics coupled with the discrete element method (CFD-DEM) demonstrate how the different operational modes can be switched in a short period of time, resulting in full local segregation in less than 40 s, without changing the fluidization air or inlet temperature. It is shown how a central spout preferentially drags big particles to the top of the bed, while a side aeration system, where two smaller spouts are opened at the outermost sides of the bed, creates a concentration of fines in the spraying region. This process can be repeated as long as the fluidization velocity of all particle sizes in the bed can be attained and full fluidization is underway. The spout regime could be used to clean the distributor plate of undesired big or overgrown particles, and side aeration to preferentially grow finer particles, while homogeneous aeration should be the default operation mode when no anomalies are detected.

1. Introduction

Fluidized bed spray granulators are widely used in the chemical industry to create high added value products such as detergents or catalyst [1] and in the food industry to improve rheological properties of bulk powders for storage or transport, with the primary example being the dosification of lactose products. For industrial applications, multi-compartment fluidized bed spray granulators are usually employed [2], given that different stages of particle growth, agglomeration, and drying can be attained by modifying chamber conditions such as spray flow rate, inlet flow and temperature [3]. The use of such systems allows for high and continuous product throughput with relatively high system flexibility to accommodate different solid hold-ups and configurations like top, side, or bottom spray [4]. However, the scale of the system and the turbulent nature of fluidization, coupled with tight product specifications, often results in relatively long stabilization times required before production can be started. For this reason, the cost of temporary shut downs due to spray clogging, overwetting of the bed, or excessive particle growth cannot be overstated, and these issues should be avoided, if possible, or corrected before reaching the point at which a shutdown might be required.

There exists a number of techniques already employed to avoid solid wetting irregularities, such as online solid water content analyzers [5], model predictive controllers (MPC) [6], population balance models (PBM) [7,8] or regular lumped heat and mass balance models, which are generally informed through CFD or CFD-DEM simulations [9]. Most of the aforementioned techniques make use of the spray rate or inlet air conditions, i.e. they alter gas temperature, gas flow rate, and moisture content. However, because most of these actuation points require changing the process parameters at least for a short period of time, they can be energetically expensive, not fit for the maximum temperature tolerances of the solid, or require long times to reach a new steady state. This work explores the possibility of adding the fluidization topology as another degree of freedom to directly affect the particle segregation, let it be for an increase of the particle size for the smaller particles or for a selective removal of the overgrown particles which could otherwise cause a shut down. To this end, a new distributor plate assembly was designed, built and tested, while CFD-DEM simulations were used to inform the design and the feasibility of the approach on a different setup. The distributor plate simply includes an air-diverting system that allows for switching from a uniform to a spouted or "inverse spouted" configuration of the bed and it is in principle suitable to be used for any device that already operates as a fluidized bed.

2. Methodology

In the present section we describe the experimental setup and the data set created with numerical simulations. The simulations were carried out with a material considered in a previous study [2], while a different substance was employed for the experiments in a larger device. The experiments and simulations were only connected via the design of the air-diverting system introduced in the distribution plate, which was tested under these two different conditions.

2.1. Experimental setup

The ProCell-25 shown in Fig. 1 consists of two wind boxes, which can be individually controlled. Depending on the amount and location of the vertical weirs in the fluidized bed, different granulation chambers can be created. In this work a single central weir was used separating the whole fluidized bed into two main chambers. In order to avoid any cross-feeding of air, each pair of wind boxes was kept at the same flow rate and temperature. With the main objective of changing the flow topology, a passive air distribution system as the one shown in Fig. 1 was designed, conceptually validated through CFD-DEM and built.

For the sake of simplicity, we analyzed the effect only on the first granulation chamber. In order to produce the type of flow topology that was required, the frame in the zoom-in cut-out in Fig. 1 separated each wind box into three sections, two wide and identical outer regions and a narrower central slot with a 4:1 ratio between the total side area and the central zone. This design decision stemmed from the CFD-DEM simulations, which showed that such a ratio would allow for a significantly better leverage over particle separation capacity due to the higher air velocities possible in the central section. The air screens required exact alignment provided by the pushing rods and tight overlapping tolerances which were obtained through a water jet cutter. In order to guarantee a homogeneous air distribution, a perforated plate was added to the top of the distribution assembly.

2.1.1. Characterization of the distributor plate

Given the number of openings that composed the air screens, it was necessary to know which fraction of the inflow was diverted to each of the sections and how linear this diversion was with the actuation distance of the rods. In addition, the flow turbulence and plate alignment created widely different velocity values just above one of the openings or if, on the contrary, the measuring system was located behind one of the fixed close sections. Thus, the flow after the diverters had to be stabilized for their calibration. 3D-printed wind channels were placed above each of the subsections of the frame as shown in Fig. 2, and a turbine anemometer (Höntzsch, Waiblingen DE) was located at the top of each wind tunnel.

After the location of the wind channels and the anemometer, the difference in velocity was measured between each chamber at different actuation distances (displacement of the supporting rods, Fig. 2(b)) and at different flow rates (Fig. 2(c)). This step was particularly critical to identify the actuation distances at which significant changes in the inlet air velocity took place and to characterize the control capacity of such an actuation.

As shown in Fig. 2(b), each of the three chambers progressively varied in velocity from 6 m/s with a fully opened central position (actuation distance 0 mm) to a value close to zero when the actuation reached 11 mm. It is worth noting that given the smaller area of the central region, the net velocity attained in this central section was significantly higher than in the side chambers, which in turn did not show a pronounced difference between the right and left chamber. Thus, we treat them as identical chambers in the following discussion. The nonlinearity and magnitude of the velocity significantly changed when increasing the inlet velocity (Fig. 2(c)) but overall the good state of the construction and chamber separation could be determined.

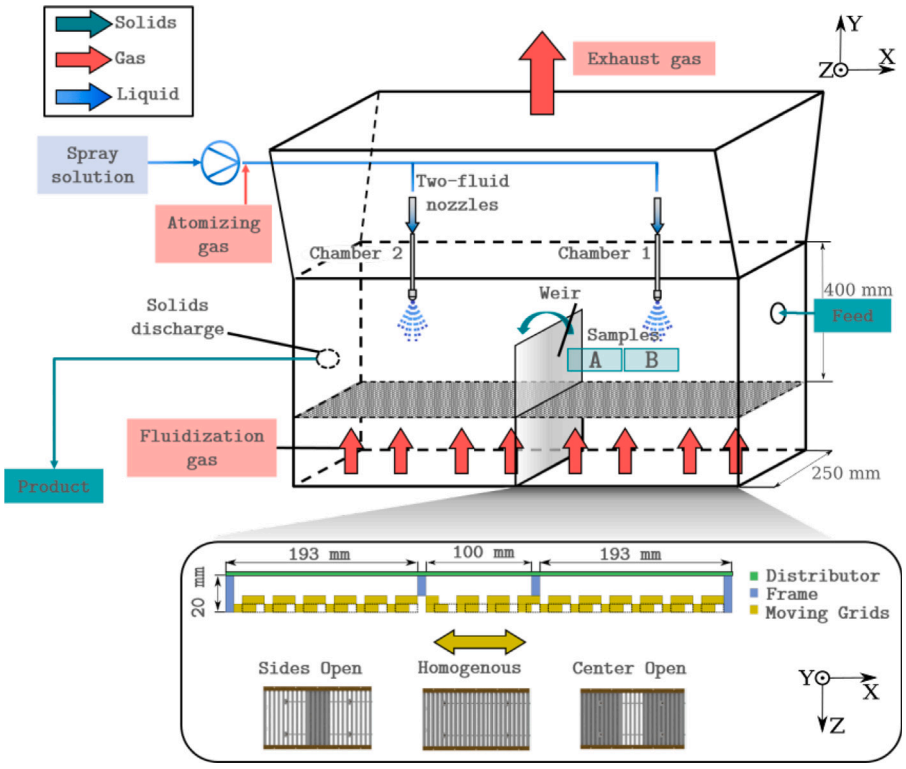

Fig. 1. Sketch of the ProCell-25 continuous granulator plant (Glatt, Binzen DE) with the top spray configuration and a continuous feed of solids and sample locations . *Source:* Adopted from [2].

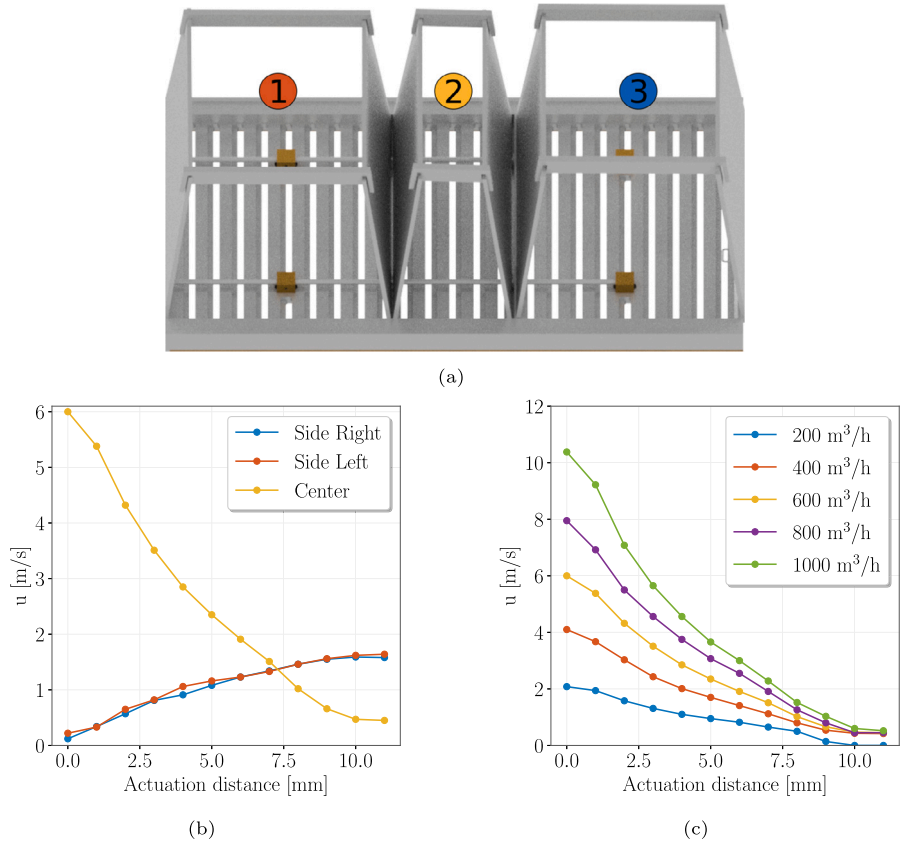

Fig. 2. (a) Wind-funnel setup, (b) corresponding variable air distribution between the chambers (for a flow-rate of 600 m^3/h), and (c) air velocity in the central channel as a function of the actuation distances for different flow-rates.

Table 1
Material properties for the particles under study.

Property	Population 1	Population 2
Average particle size, [μm]	1000	2100
Standard deviation, [μm^2]	1.25	1.25
Particle density, ρ_s [kg/m^3]	2500	
Bulk density, ρ_b [kg/m^3]	1800	
Type	Geldart B	
Minimum fluidization velocity, u_{mf} [m/s]	0.56	1.07

2.1.2. Analysis of segregation and particle size distribution

In order to analyze the effect of flow topology in particle segregation, a bed composed of an equi-volumetric binary particle mixture was created . Table 1 provides its basic properties including the minimum fluidization velocity u_{mf}, which was computed for each population using the Ergun equation with the average diameter and the volume fraction of loose random packing of about 0.40. For the control to work as intended, the homogeneous flow rate had to be sufficiently large to reach at least a certain degree of fluidization, so that the inflow for the high-velocity patches in control cases was automatically well above the minimum fluidization velocity.

During experiments, the flow topology was varied and solid samples were drawn out from the points denoted A and B in Fig. 1 with an iso-kinetic solid sampler. These samples were then off-line analyzed through a Camsizer XT (Retsch, Hann DE) which captured high-speed pictures of the sampled particles and estimated the particle size according to the shadow projected to the camera. In order to reduce uncertainty and guarantee that they were representative of the state of the system, three samples were drawn out of the device for every experimental point, which allowed to assess their variance. It is also worth noting that any disturbance on the overall particle population by the sampling process was minimized by extracting no more than 50 mg per sample in a bed of 15 kg and allowing enough time for the bed to settle and mix again the sampling point. This was confirmed by the small variance of the measured values.

2.1.3. Optical setup and analysis

To obtain optical access for experimental validation, the front metal plate of the ProCell 25 was replaced by an anti static PMMA plate (Koenig, Karlsruhe DE). The optical setup consisted of two continuous current high-intensity lamps (Dedo Weigert Film GmbH, Munich DE) and a black-and-white high-speed camera (NX-S2, Imaging Solutions GmbH, Eningen DE) that was able to record up to 4000 fps at full resolution (1024 × 1024 px). In order to homogenize the lighting and remove any hard reflections in the scene, both light sources were equipped with diffusers.

For the validation experiments no spraying was used in order to simplify image capture and improve picture quality. It is clear from the rectangular geometry of the ProCell 25 that there was no optical access across the entire bed width, and the analysis of particle velocities was restricted to the near-wall region close to the front plate. The calculated particle velocities were obtained from cross-correlation based particle image velocimetry (PIV) processing conducted in Davis 10 (LaVision, Goettingen DE). The vector fields were calculated with an iterative grid refinement and a final window size of 16 × 16 pixels.

Once the capture of a given fluidization regime was conducted, the footage was processed through Matlab in order to detect the average particle velocity for each region of interest and overall flow topology. Given the time required for data transfer and image treatment, processing was conducted off-line.

2.2. Numerical setup and data set

We performed CFD-DEM simulations using the CFDEMcoupling implementation [10,11], which consists of the finite-volume library OpenFOAM [12] coupled with the DEM code LIGGGHTS [13]. The latter is based on the LAMMPS library for molecular dynamics calculations [14]. In these simulations, OpenFOAM describes the fluid phase (air) by solving the incompressible Navier–Stokes equations for a porous medium, while LIGGGHTS handles the solid phase (product particles). The coupling effects between fluid and particles are described by the force exerted by the fluid over each particle, by the porosity, and by the interfacial momentum-transfer term in the Navier–Stokes equations.

Following Anderson and Jackson [15], the governing equations for the gas phase take the form

$$\frac{\partial \alpha}{\partial t} + \nabla \cdot (\alpha \boldsymbol{u}) = 0 \tag{1}$$

$$\frac{\partial (\alpha \boldsymbol{u})}{\partial t} + \nabla \cdot (\alpha \boldsymbol{u}\boldsymbol{u}) = -\alpha \nabla \left(\frac{p}{\rho}\right) + \nu \alpha \nabla^2 \boldsymbol{u} - \frac{1}{\rho V} \sum_{k=1}^{n_p} \boldsymbol{F}'_k \tag{2}$$

In these expressions, $\boldsymbol{u}$, α, ρ, and ν denote, respectively, the gas velocity components, volume fraction, density, and kinematic viscosity; V is the volume of the local cell, and $\boldsymbol{F}'_k$ the particle–fluid interaction for particle k *without pressure and viscosity contribution*. In the present case, it consisted only of the drag force, which was computed using the correlation proposed by Beetstra et al. [16]. The particle governing equations solved in LIGGGHTS are Newton's equations of motion, where the total force and torque acting on each particle are the sum of the force and torque caused by the fluid and by the neighboring particles, as described by Kloss et al. [13]. In particular:

$$\frac{\mathrm{d}}{\mathrm{d}t} \boldsymbol{x}_i = \boldsymbol{v}_i \tag{3}$$

$$\frac{\mathrm{d}}{\mathrm{d}} (m_i \boldsymbol{v}_i) = \sum_{j \neq i} \boldsymbol{F}_{j \to i} + \boldsymbol{F}_i + m_i \boldsymbol{g} \tag{4}$$

$$\frac{\mathrm{d}}{\mathrm{d}t} (\boldsymbol{J}_i \boldsymbol{\omega}_i) = \sum_{j \neq i} \boldsymbol{T}_{j \to i}\,, \tag{5}$$

where $\boldsymbol{x}$ and $\boldsymbol{\omega}$ are the particle position and angular velocity, respectively, m is the mass, $\boldsymbol{J}$ is the inertial momentum, $\boldsymbol{F}_{j \to i}$ and $\boldsymbol{T}_{j \to i}$ are, respectively, the force and torque exerted by particle j to i, $\boldsymbol{F}_i$ is the total force caused by the fluid on particle i, and $\boldsymbol{g}$ is gravity.

We employed a reference system, where x denotes the horizontal direction parallel to the hypothetical direction of product migration in the bed, y the vertical direction, and z the second horizontal direction. The corresponding instantaneous velocity components for the fluid are denoted by u, v, and w. The setup we considered was not designed to reproduce the experiment, which was an industrial-scale system and would have required significant computational resources, but rather to represent the main control effects in a smaller test case that did not require coarse-graining or additional modeling. In particular, we employed a simplified geometry with a size that was reduced by a factor of approximately 2.5 in both horizontal directions, so that the domain extended for 0.2 m and 0.1 m in x and z. Furthermore, the total mass of the bed in the simulations was limited to 1 kg, and we considered a bidisperse particle distribution where the classes of larger and the smaller particle had a diameter of $d_1 = 2 \times 10^{-3}$ m and $d_2 = 4 \times 10^{-3}$ m, respectively. Both particle classes were assigned 50% of the total mass of the bed, resulting in a total of approximately 93 000 particles. A comprehensive description of the numerical setup is reported in Table 2.

These numerical simulations aimed to describe the impact on segregation of an air-diverting system similar to that employed in the experiment. To this end, we created a relatively large data set including (i) reference cases which differed for the total air flow as well as (ii) controlled cases, where a non-uniform inflow was used as a model for the air-diverting system. The non-uniform inflow in the control cases was obtained by splitting the air inlet into three different patches with the same proportions as in the experiments, i.e. the side patches were twice as long as the central patch. Due to the different areas of the side and central patches, it was possible to obtain a larger

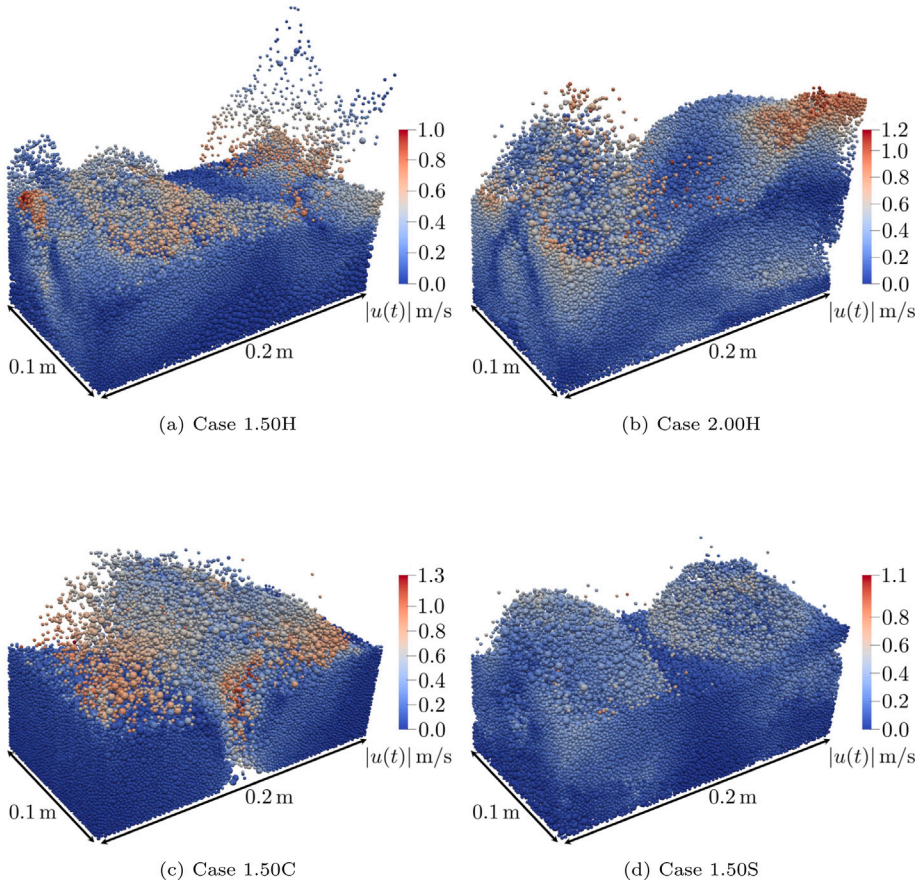

Fig. 3. Particle velocity magnitude for four of the considered cases. Domain and particle sizes are to scale, and the notation of case names equals that in Table 3.

Table 2
Setup of the simulation for (top) OpenFOAM and (bottom) LIGGGHTS. Material properties are the same as the in study by Diez et al. [2].

Number of cells	80 000
$\Delta x = \Delta y = \Delta z$ [mm]	5
Δt_{CFD} [s]	$2.5 \cdot 10^{-5}$
ρ [kg/m^3]	1.189
ν [m^2/s]	10^{-5}
Number of particles	93 254
Particle diameters [mm] (class 1 & 2)	2 & 4
Δt_{DEM} [s]	$2.5 \cdot 10^{-6}$
g [m/s^2]	9.81
ρ [kg/m^3]	1440
u_{mf} [m/s] (class 1 & 2)	0.75 & 1.2
Young modulus [GPa] (particle & wall)	1.58 & 180
Poisson ratio (particles & wall)	0.22 & 0.3
COR (particle–particle & particle–wall)	0.55 & 0.55
Sliding friction coeff. (particle–particle)	0.8693
Sliding friction coeff. (particle–wall)	0.0981

range of air velocities in the central patch for a given total influx. It could vary from 0 to 5 times the inflow velocity of the uniform case, while the inflow velocity on the side patches could vary only from 0 to 1.25 times that of the uniform case. We focused on two control configurations: in the first configuration, denoted by central actuation (C), the side patches of the inlet were partially obstructed so that only half of the nominal inflow passed through them; in the second configuration, denoted by side actuation (S), the central patch of the inlet was completely obstructed, so that the entire nominal inflow was forced through the side patches. A complete list of the cases examined in this work, including the inflow velocity for the different patches, is reported in Table 3. Similar to the experiment, the control was supposed to act on a reference case for which fluidization had been reached by changing the circulation patterns in the system. Hence, the specific relation between inflow velocities and e.g. u_{mf} or other properties of the bed were not investigated. The same workflow was adopted for all cases. The initial condition consisted of a cloud of particles with random locations in the domain and the fluid at rest. The inflow velocity was 0 at $t = 0$ s and it reached the values indicated in Table 3 at $t = 0.2$ s. A transient of $t = 2$ s from the initialization was excluded from all cases to assure a certain degree of independence from the initial condition, longer transients were however apparent for some inflow configurations and the simulation time after this transient was not the same for all cases, as discussed later. Visualization from arbitrary time steps of a selected portion of the data set are provided in Fig. 3.

3. Results

3.1. Effect on flow topology

In the first run of experiments, the inlet flow rate was modified from a minimum of 200 m^3/h (0.85H) to a maximum of 1000 m^3/h (4.2H). The resulting flow was recorded with the high speed camera to determine its overall qualitative topology at each actuation mode as displayed in Fig. 4.

The first result obtained from these experiments was the clear change in topology at fixed air flow rates for each aeration mode. Within a given aeration mode, comparing Figs. 4(a) –4(c) with Figs. 4(d)–4(f) evidences that no significant changes were observed when increasing the flow rate other than a higher bed expansion and overall spout height for Fig. 4(f) relative to Fig. 4(c), where the bed was more turbulent and better mixed at higher flow rates.

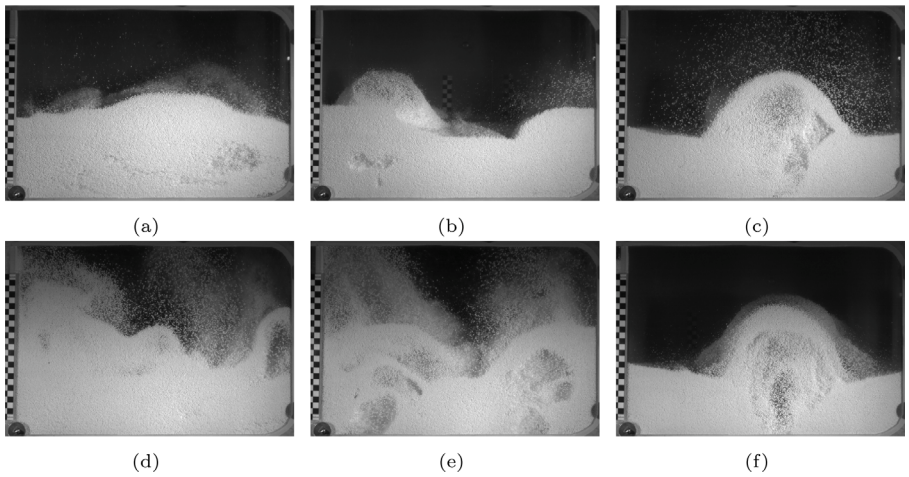

Fig. 4. Selected images from the high speed camera for (a) homogeneous, (b) side, and (c) central aeration at 400 m^3/h (1.70H, 1.70C, and 1.70S respectively), and (d) homogeneous, (e) side, and (f) central aeration at 600 m^3/h (2.60H, 2.60C, and 2.60S respectively).

Table 3
List of cases considered in the present study. Note that u_{S1}, u_C, and u_{S2} denote, respectively, the inflow velocity over the inlet patches on the left, in the center, and on the right. The control cases are grouped together with the corresponding reference case with the same total inflow. The inflow velocities for case 1.50T are not uniform in time and are described later in the paper.

Case name	u_{S1} [m/s]	u_C [m/s]	u_{S2} [m/s]
1.25H	1.25	1.25	1.25
1.25C	0.625	3.75	0.625
1.25S	1.5625	0	1.5625
1.50H	1.50	1.50	1.50
1.50C	0.75	4.5	0.75
1.50S	1.875	0	1.875
1.50T	–	–	–
1.75H	1.75	1.75	1.75
1.75C	0.875	5.25	0.875
1.75S	2.1875	0	2.1875
2.00H	2.00	2.00	2.00

Regarding the flow topologies, the homogeneous aeration configurations shown in Figs. 4(a) and 4(d) led to a massively unsteady behavior where bubbles rose up throughout the bed in a turbulent manner. However, when the center region was closed and air was only directed through the sides, two clear, permanently bubbling (at low flow rates, cf. Fig. 4(b)) and fluidized (at higher flow rates, cf. Fig. 4(e)) spout regions were created. The center remained relatively calm as particles moved downwards in the bed. When the whole flow was directed through the center as displayed in Figs. 4(c) and 4(f), a vigorous spout was well fixed at this location. Considering the reduced cross-sectional area of the center region relative to the sum of both side chambers, the spouted particle velocity was significantly higher, which highlights the ability of this configuration to reset or clear the distributor plate.

The well-defined heterogeneous fluidization of the center and side aeration configurations called for a quantification of the particle velocities through external PIV as provided in Fig. 5. These average particle velocity fields clearly demonstrate the difference between the center and the side aeration configurations. In the former case displayed in Figs. 5(a) and 5(c), a small center region with particle velocities ranging between 0.5–1 m/s can be seen, while the sides show a wider, downward moving, solid region characteristic for spouted beds [17] or spouted-bed-like systems [18]. When only the side inlets were open at low velocities, slight upwards moving regions visible in Fig. 5(b) emerged at both sides but with an overall homogeneous, rather low bed height. However, increasing the flow rate consistently made these regions more pronounced as evidenced by Fig. 5(d). These measurements confirmed the impression of fluidization topology changes obtained from snapshots like Fig. 4 due to actuation of the air distributor plate.

It is worth noting that the experimental setup could be prone to some errors in solid velocity measurement, such as the friction of the frontal wall or the incorrect particle velocity detection due to lighting conditions or particle sizes. Thus, simulations became of foremost importance not only to confirm the qualitative findings of the experiments, but also to create the perfect environment to infer the influence of process parameters on particle velocity or segregation. Lastly, they also provided valuable 3D data, which are hard to obtain experimentally.

Therefore, we examined control effects on particle fluidization in the simulated cases. We first provide the definition of the averaging operator for particle-related quantities that are employed hereafter, using the velocity as an example. The particle velocity is defined as a mass-weighted average for each cell:

$$\overline{v_m}(\boldsymbol{x}) = \frac{1}{M}\int_{t^*}^{t}\sum_{j=1}^{n_p(\tau)} m_j v_{p,j}(\tau)\,\mathrm{d}\tau\,. \tag{6}$$

In this expression, t^* and t denote the initial and final time steps of the average interval, respectively, $n_p(\tau)$ denotes the particle number in cell $\boldsymbol{x}$ at time τ, and $M = \int_{t^*}^{t}\sum_{j=1}^{n_p(\tau)} m_j \mathrm{d}\tau$. Furthermore, the right and left halves of the domain, which were equivalent because of the symmetry with respect to plane $x = 0.1$ m, were averaged together to improve convergence. We adopted this definition instead of an unweighted time average of the Eulerian granular velocity field in the CFD-DEM simulation because it is more similar to that obtained from PIV measurements. The solid-phase velocity in a CFD-DEM simulation vanishes in empty cells, introducing a bias in the average. On the other hand, for a mass-weighted average, statistical convergence is progressively worse moving towards the edge of the bed, and it is not defined in cells never visited by particles in the considered time interval.

The control effects on the flow topology are illustrated in Fig. 6 in terms of the mass-averaged horizontal and vertical components of the velocity $\overline{u_m}$ and $\overline{v_m}$ in the center plane. The vertical velocity component was directly impacted by the control. Beyond the qualitative observation that a higher fluidization rate corresponded to higher $\overline{u_m}$ and $\overline{v_m}$, particle velocity components did not give direct indications on the height of the fluidized bed. To provide information on how the control affected the particle distribution, we superimposed contours corresponding to an average value of 0.5 of the solid volume fraction to Fig. 6.

We focused on the cases with the same total inflow as 1.50H because this intensity led to an intermediate state for which there was still a

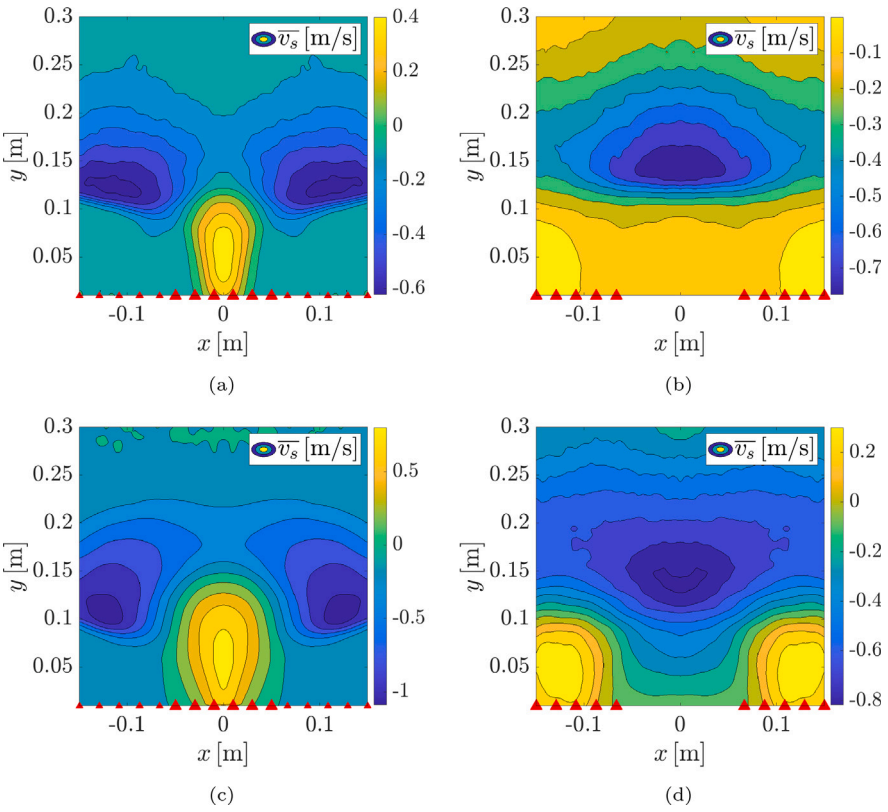

Fig. 5. Experimental PIV measurement of the average vertical particle velocity for: (a & b) center and side aeration at 400 m^3/h (1.70C and 1.70S) and, (c & d) for center and side aeration at 600 m^3/h (2.60C and 2.60S). The red triangles highlight the inflow strength.

significant degree of segregation built up after progressive deposition over a long time scale, while also having a relatively high degree of fluidization. It can be seen in the next section that case 1.25H was most likely too far from a realistic operation mode, and in 1.75H and 2.00H segregation was less evident.

In the reference (1.50H), both mean particle velocity components were quite low in absolute value, owing to the absence of any mechanism that could cause a strong circulation in the bed. The change of sign for the horizontal mean velocity was a consequence of wall effects, as particles moved with a slight prevalence towards the center in the corner region of the domain and from the center towards the sides elsewhere.

In case 1.50C, where the air-diverting system effectively caused the bed to operate in a spouted-like configuration, it was possible to clearly identify the region of high positive vertical velocity above the central patch, and the presence of a counter-clockwise and a clockwise mean circulation motion in the left and right half of the domain, respectively. The high velocity in the center also led to the formation of large air bubbles in this region and thus a lower solid volume fraction. To the contrary, the average particle velocity was particularly low in the proximity of the domain corners.

Lastly, in case 1.50S, where the central portion of the inlet was sealed, two circulation patterns appeared in the side regions. Due to the presence of the walls, the average particle movement was opposite to that in the previous case. In particular, particles moved from the side to the center in the upper portion of the bed, but from the center to the side in the lower portion.

3.2. Particle segregation

In addition to changing the overall flow topology, the question still remained of whether this change resulted in a significant modification of the local particle segregation at the top of the bed. To provide experimental evidence, samples were drawn at 400 m^3/h from the top of the bed for each configuration, i.e. homogeneous aeration, side and center aeration respectively. The corresponding particle size distributions (PSDs) above the side and the center chamber are provided by Figs. 7(a) and 7(b), together with the value of the Sauter diameter

$$d_{32} = \frac{\sum_i d_i^3}{\sum_i d_i^2}, \tag{7}$$

which represents the diameter of a hypothetical particle with the same ratio between volume and surface of the particle cloud.

Fig. 7(a) shows that the PSDs on the sides were hardly modified when a control configuration was employed. However, when analyzing the samples of the center point, which is of most interest in the granulation process, a very significant change was identified between the two control cases in Fig. 7(b). When the center of the chamber was opened in a spout-like configuration, more coarse particles were found on the top of the bed as the air in this region surpassed the minimum fluidization velocity of both particle populations. In contrast, when both sides were open and the center closed, this phenomenon took place at the sides, while the center allowed for fine particles to percolate through the bed and accumulate at the top of the bed, even at high flow rates.

Therefore, when an anomaly is found where a population with smaller size is present in the PSD, a momentary or pulsed side opening is recommended, so as to granulate or coat these fine particles preferentially. The center opening configuration, on the other hand, might be used to clean the distributor plate of overgrown particles that might cause the eventual shut down of the operation. Once the fine particles have been grown to the normal average particle size of the rest of the PSD or the overgrown particles have been pushed out, the system can revert to an homogeneous operation. It is worth noting that in our investigation, this onset of segregation already happened in the first 30 s after actuation. Therefore, an operation that switches between these regimes could be beneficial.

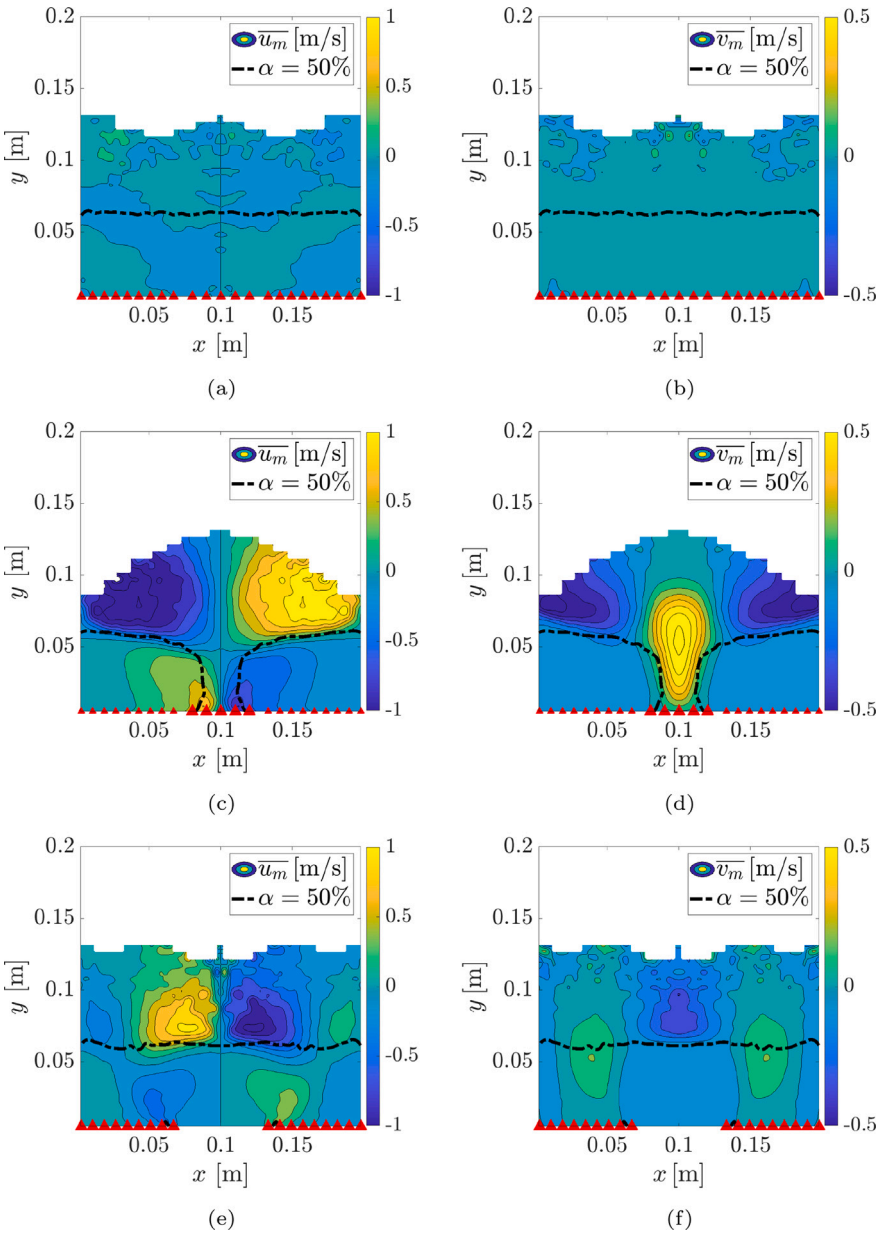

Fig. 6. Mass-weighted average particle velocity on plane $z = 0.05$ for: the reference case (a & b), actuation in the center (c & d), and on the side (e & f). Horizontal and vertical velocity components on left and right column, respectively. The dashed black lines denote a value of average volume fraction of 50%. The red triangles are a visual clue for the different inlet conditions.

In the experiments, segregation could be measured reliably only at the top of the bed due to the uncertainty of drawing samples from within the bed. However, simulations allow for a great spatial and temporal look at the evolution of segregation. Thus, we provide simulation results for the four reference cases. In particular, we present the time evolution of the vertical coordinate of the center of mass and the mean probability density function (PDF) in the vertical direction shown in Fig. 8 for the two particle classes. The vertical coordinate of the center of mass, denoted by y_{cm}, is defined for each size class as

$$y_{\mathrm{cm}}(t) = \frac{1}{N}\sum_{i=1}^{N} y_i(t)\,, \tag{8}$$

where N is the number of particles of the corresponding diameter. The grain mass does not enter this definition because all particles within each of the two separate size classes have the same mass. The PDF in the vertical coordinate is defined based on a given binning distribution which is the same for all cases to allow for a direct comparison, and it is normalized so that $\int \mathrm{PDF}(y)\mathrm{d}y = 1$. We focused on these two quantities rather than a segregation index because they provide more precise indications about both segregation and fluidization state. The center of mass $y_{\mathrm{cm}}(t)$ was computed with a relatively high sampling rate to give a qualitative indication of the characteristic time scales of the system. The mean PDF was obtained over a certain time interval where we assumed at least qualitative statistical stationarity, i.e. conditions where averaged quantities depend only on the length of average interval and not on the instant selected to start sampling. We believe that a more precise characterization of each regime in this model test case was not necessary for the purpose of the present work.

The four different reference cases illustrate how the total inflow led to different fluidization regimes, which also affected the time scale and the dynamics with which segregation occurred. In case 1.25H, the lowest total inflow of the data set, we observed a progressive deposition of the larger particles in the lower portion of the bed, which occurred with a relatively long time scale with respect to the instantaneous

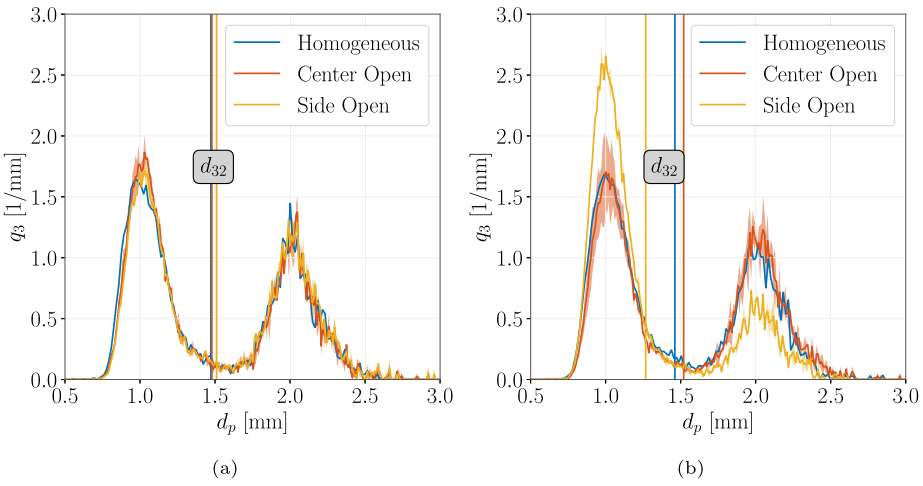

Fig. 7. PSD for samples taken at (a) sides of the bed and (b) center of the bed for homogeneous, center-open and side-open flow topologies.

fluctuations of the center of mass. In case 1.50H, progressive deposition also took place but with an even longer time scale, and we began to observe larger fluctuations that temporarily increased segregation between smaller and larger particles over a period of many seconds. In both 1.75H and 2.00H, the total inflow was high enough to limit progressive deposition of the larger particles and the system appeared to be fully chaotic. In case 2.00H, the inflow intensity was enough to almost remove segregation, even though there was still an increase in the concentration of larger particles in the lowest region of the domain.

The time evolution of y_{cm} for the reference cases may suggest that a well-defined statistically stationary state had not been reached yet because time scales comparable with the average time were still present, but we chose to compute the average PDF nevertheless for the sake of simplicity. This choice was justified by the fact that, as we shall see later on, one of the control effects was to disrupt the very long time scales that were active in the reference cases. Our results also provide an estimate of the variation of inflow intensity that is needed to have appreciable effects on segregation, if the total inflow velocity is the sole control parameter.

As shown Fig. 6, statistically stationary conditions in the control cases were established as a result of the equilibrium between transport in regions of the domain with high solid volume fraction and low particle velocity, and regions with low solid volume fraction and high particle velocity. This mechanism was directly connected with control effects on segregation. We investigated how inflow distributions affected the bed dynamics using the vertical coordinate of the center of mass for larger and smaller particles and the mean PDF of the particle vertical coordinates displayed in Fig. 9. Centers of mass and PDFs were computed separately for both the center and side regions of the domain. In the reference case, these quantities were in good agreement in both regions, showing segregation and the slow deposition process of larger particles, as discussed before. Controls effects are clearly visible in both the center and the side regions. The two cases with control still exhibited a certain degree of segregation over the inlet patches with the more intense inflow, i.e. the center patch for case 1.50C and the side patches for case 1.50S. In the regions corresponding to patches with lower inflow intensity, for both control configurations, smaller particles percolated to the bottom of the bed resulting in a regime where the average center of mass and the location of higher concentration were at a higher location for larger particles. This "inverse segregation" is typically a consequence of the granular demixing that occurs in agitated containers, where larger particles eventually float over smaller ones [19]. In the cases considered here, the presence of adjacent portions of the bed with different flow rates had a similar effect on the regions where fluidization was not sustained. The condition of inverse segregation was particularly evident in the side regions of case 1.50C. Another control effect that was apparent from the time evolution of the average center of mass was the disruption of the long-timescale motions present in the reference case, which were substituted by the clockwise and counter-clockwise circulation patterns shown in Fig. 6.

Lastly, to summarize control effects on particle distribution, we examine the mass-weighted time-averaged Sauter mean diameter $\overline{d_{32}}$ for all cases in Fig. 10, which directly highlight regions with particle deposition. In the reference cases, the relatively high $\overline{d_{32}}$ in the lower portion of the fluidized bed was a consequence of the progressive deposition of larger particles, which had a higher volume/surface ratio. In control cases with more intense inflow from the center patch, it was possible to identify the concentration of smaller particles in the domain corners. In control cases with more intense inflow from the side patches, segregation was still present and therefore there was deposition of larger particles over the control patches, while also having a higher concentration of smaller particles over the lower inflow in the center.

The segregation of a given population is heavily dependent on their relative minimum fluidization velocities and buoyancy forces. An experimental analysis of the local segregation at different flow rates was also conducted as to identify possible limitations of the system. Thus, the inlet fluid velocity was increased and particles were extracted from the top of the bed at a central location and above each of the sides. Fig. 11 compares their Sauter mean diameter with the system-wide average. As expected, the inlet flow rate strongly affected the mean particle diameter on top of the bed for all configurations. For homogeneous aeration as shown in Fig. 11(a), the difference between the center or a side location was negligible at high flow rates as the bed was well mixed and random bubbling behavior was expected not to lead to significant particle segregation. However, at low flow rates a significantly lower particle size was found on top of the bed in both center and side location as the fine particles floated to the top of the bed and coarse particles sank down to the distributor bed. In this regime, however, no real fluidization took place, and it is therefore usually discarded from operation.

When the center spout was created and all the air was directed through the center, Fig. 11(b) demonstrates the same phenomenon at low flow rates, where fine particles were preferentially found at the top of the bed. However, as the flow rate and hence the air momentum increased, coarse particles were found preferentially at the center location than at the sides. This trend was confirmed for all flow rates. But as previously stated, the most interesting regime, from a granulation perspective, was the side aeration configuration, Fig. 11(c), where smaller particles were found at the center of the bed for all flow

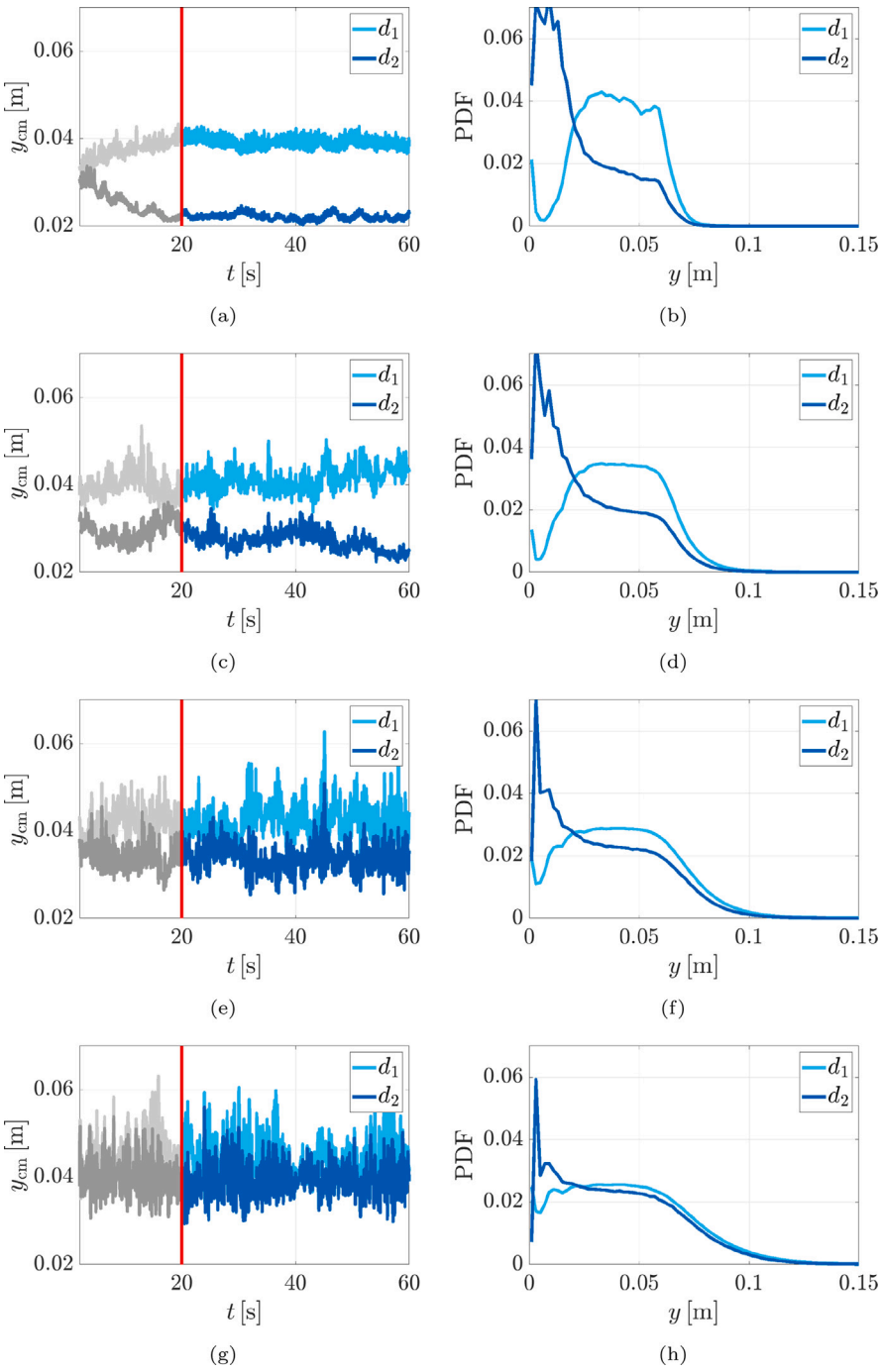

Fig. 8. (Left column) Vertical coordinate of the center of mass and (right column) PDF of the vertical particle coordinates for d_1 and d_2 in cases 1.25H (a & b), 1.50H (c & d), 1.75H (e & f), and 2.00H (g & h). Red vertical lines denote the starting average time, $t^* = 20$ s.

rates once the air had enough momentum to fluidize all the populations contained in the bed. This phenomenon might be explained by the fact that at each of the sides, coarse particles were being dragged-up the bed while finer particles percolated or floated to the center, where the granulation spray is usually located, predictably increasing the size of these particles in a preferential manner.

Thus, it was simulated and experimentally confirmed that segregation happened on top of the bed for each controlled case at high flow rates and that it could be controlled. However, its time dependency still needed to be inferred for our approach to be applicable. Therefore, we carried out simulations picturing the transition behavior of segregation for the different control scenarios.

3.3. Transient segregation behavior

The first advantage of implementing an air-diverting system as described in the present paper is the capacity of controlling the degree of segregation above the different patches. A second advantage, perhaps even more significant, is the capacity of modifying the rate at which particles move across the bed. Even though we did not consider any over-imposed drift with particle injection and extraction, which would be the typical operation mode for the device considered in the experiment, we were still able to investigate control effects on the lateral mixing process. To this end, we introduced the proportion of particles that moved at least once from the left half to the right half of the domain, or vice-versa from the right half to the left half, in a given

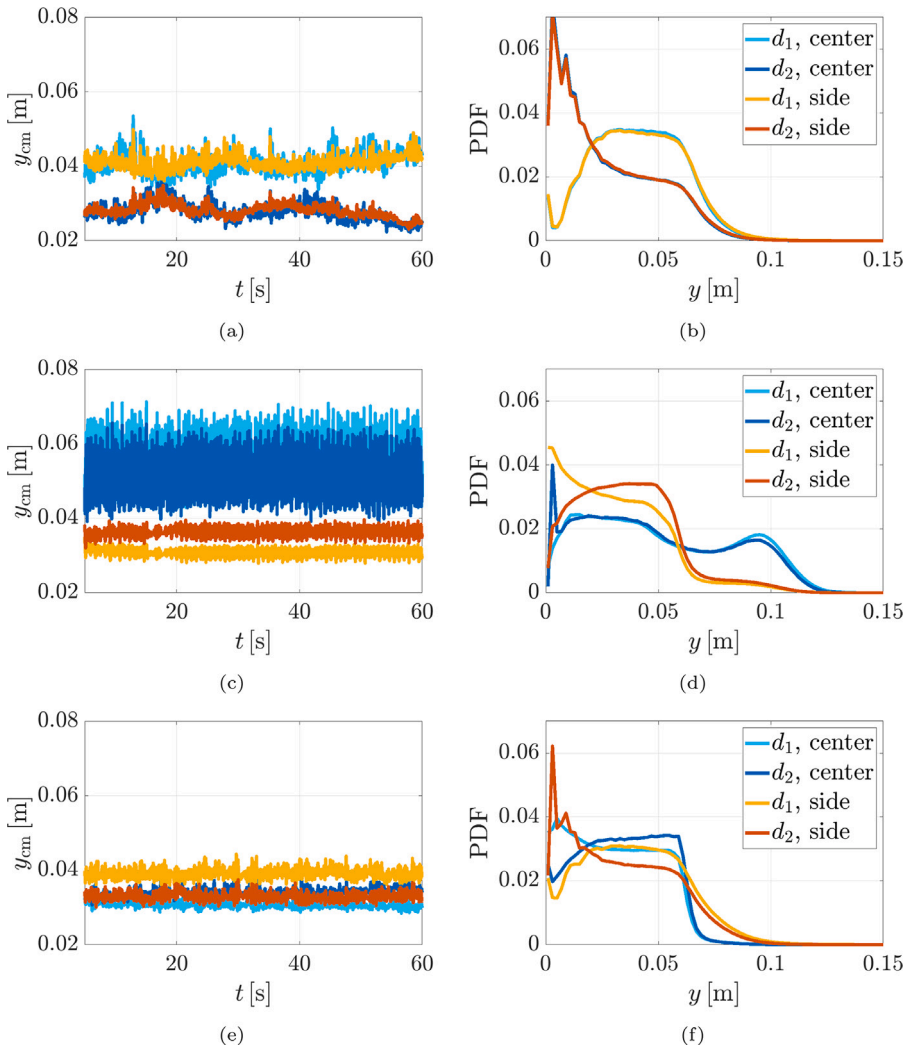

Fig. 9. (Left column) Center of mass of both particle classes and (right column) PDFs of the particle vertical coordinates, for cases 1.50H (a & b), 1.50C (c & d), and 1.50S (e & f).

time interval. This quantity, denoted by $P_{L\leftrightarrow R}$, is suited to describe the global mixing in the bed because it does not take into account the fact that particles with an initial position close to the mid-plane of the domain may migrate from one side to another multiple times in the same interval that is required for particles with an initial position close to the left or right wall. The proportion of migrated particles $P_{L\leftrightarrow R}$ is shown in Fig. 12 for the reference cases and the controlled cases with the same total inflow as case 1.50H. Both the change of total inflow and control actuation had a strong impact on this quantity.

For all cases considered here, $P_{L\leftrightarrow R}$ was computed from $t^* = 20\,\mathrm{s}$ to $t = 60\,\mathrm{s}$, which was the same interval for which statistics were sampled, and was evaluated separately for larger and smaller particles. In general, the common trend that $P_{L\leftrightarrow R}$ exhibited was the same, i.e. it monotonically increased from 0 to 1, as all particles would eventually move across the mid-plane $z = 0.1\,\mathrm{m}$ for the first time. However, there was a significant difference in the time scale with which this process occurred in the various cases. In uncontrolled cases with a relevant degree of segregation, larger particles were relatively stationary in the lower portion of the bed. In 1.25H in particular, less than 40% of the larger particles had changed the domain side at least once even after 40 s of simulated time, and in 1.50H still 20% had not changed domain side in the same time. Smaller particles were more mobile than larger ones unless in 2.00H, for which segregation was not occurring, and in this last case $P_{L\leftrightarrow R}$ was in good agreement between both particle classes.

Control effects on global mixing were virtually opposite for the two control strategies. In 1.50C, $P_{L\leftrightarrow R}$ became higher than in the corresponding reference case, and it was also higher for larger particles than for smaller ones. The higher mobility of larger particles was due to the percolation of smaller particles in the corners of the domain, which has already been discussed in the previous section. Nevertheless, even for smaller particles $P_{L\leftrightarrow R}$ was still higher than in the reference case, and it still converged to approximately 1. Despite the presence of inverse segregation, the large circulation pattern induced by the control allowed the smaller particles to migrate to the opposite side with relative ease. In 1.50S, $P_{L\leftrightarrow R}$ was lower than 1.50C and in fact even lower than in the reference case. This apparently counter-intuitive result, given the two opposite circulation patterns, was caused by the low fluidization in the center region impeding migration in the horizontal direction.

We have so far considered those cases where inflow conditions remained constant over a relatively long period of time, at least of the same order of magnitude with the longer time scales active in the system. Lastly, we present case 1.50T, which was designed to discuss how the air-diverting system can modify the bed when different inflows are cycled through with a predetermined sequence. In particular, the homogeneous mode of operation was maintained for the first 10 s, followed by 10 s with center actuation, 10 s with side actuation, and then reverting to homogeneous inflow. The time of transition between operation modes was 1 s, which was a conservative estimate based on

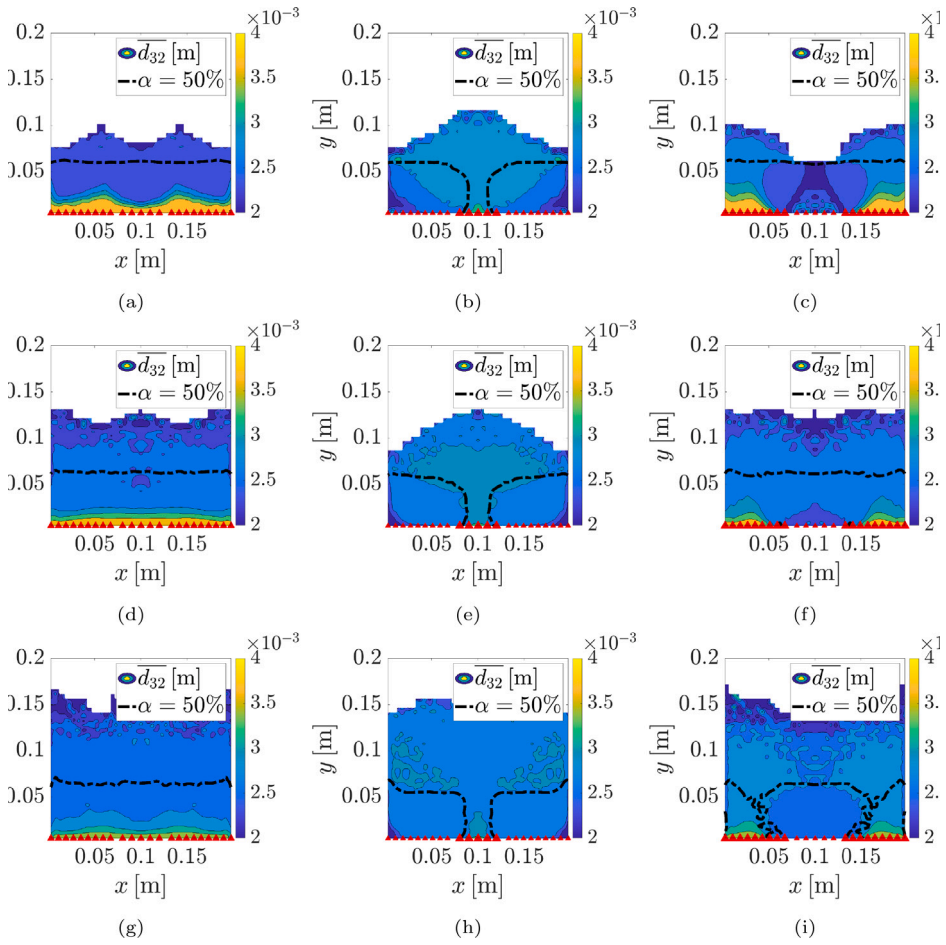

Fig. 10. Mean Sauter diameter for, from top to bottom: cases with the same total inflow of (a-c) 1.25H, (d-f) 1.50H, and (g-i) 1.75H and, from left to right, (a, d, g) the reference cases, and cases with center (b, e, h) and (c, f, i) side actuation.

our experience operating the air-diverting system in the experimental setup. In Fig. 13, we show the effects of switching between aeration modes on the time evolution of both particle classes in case 1.50T, as well as on $P_{L\leftrightarrow R}$ measured for an initial time of $t^* = 1$ s. These are contrasted with the same quantities for case 1.50H, which have been shown before. The bed adjusted virtually instantaneously to the new inflow conditions for what pertained to the average height of the bed and fluctuation amplitude. Even though this was an expected result, given the very fast time scale of the interaction between neighbors particles, it further highlights the fundamental benefit of employing an air-diverting system as the one proposed in this paper, because the bed itself was indeed capable of reacting to a relatively fast actuator. At the same time, the transition from one operation mode to another with the time scale prescribed here also stopped the slow deposition processes which have been described previously. This interruption was observed, firstly, as a short-term effect in the transition between one mode to another in case 1.50T and, secondly, as a long-term effect comparing the states of the bed with control cycle with those for homogeneous inflow conditions.

A second interesting consequence of the cycling between the operation modes was the increase of $P_{L\leftrightarrow R}$ for larger particles. It was caused by the activation of the spouted mode, which was however combined with a similarly high $P_{L\leftrightarrow R}$ for smaller ones. Due to the fact that the proportion of migrated particles is a global measure of the degree of mixing in the bed, its increase for both classes was not limited to the portion of flow history where the control was active, and therefore we achieved in case 1.50T that $P_{L\leftrightarrow R}$ was in good agreement between larger and smaller particles. The only other configuration for which we observed that the two particle classes had a similar probability of migration from one side to the opposite of the bed was 2.00H, illustrating again how a localized change of inflow conditions can have effects similar to those of a significant increase of total flow rate.

4. Conclusion

The design, construction and validation of a new air distributor plate for a multi-compartment spray granulator was conducted, where a significant change in the flow topology was almost instantaneously attained for flow rates up to 800 m^3/h. CFD-DEM simulations of a smaller model resembling e.g. a top-down spray configuration with a fine population in the PSD showed a direct link between these modifications of the flow and different regimes of particle segregation, which was also observed in the experiment.

The comparatively simple nature of our control mechanism allows it to operate effectively on a wide range of flow rates. The only practical constraint for its implementation is that the base case is working with a reasonable degree of fluidization, which is the standard operating condition of many reactors. In this case, the higher velocity reached in the corresponding patches when the control is active will also be sufficient to maintain fluidization, having the desired effects on the recirculation pattern in the bed that we described in the previous section. In particular, the side aeration configuration provided for a local accumulation of fines in the central region of the bed without the need to change the air flow rate. On the other hand, the center aeration and subsequent spout regime created the opposite effect with bigger particles being more prevalent in the central region. The evolution of particle segregation was experimentally confirmed for a wide range of

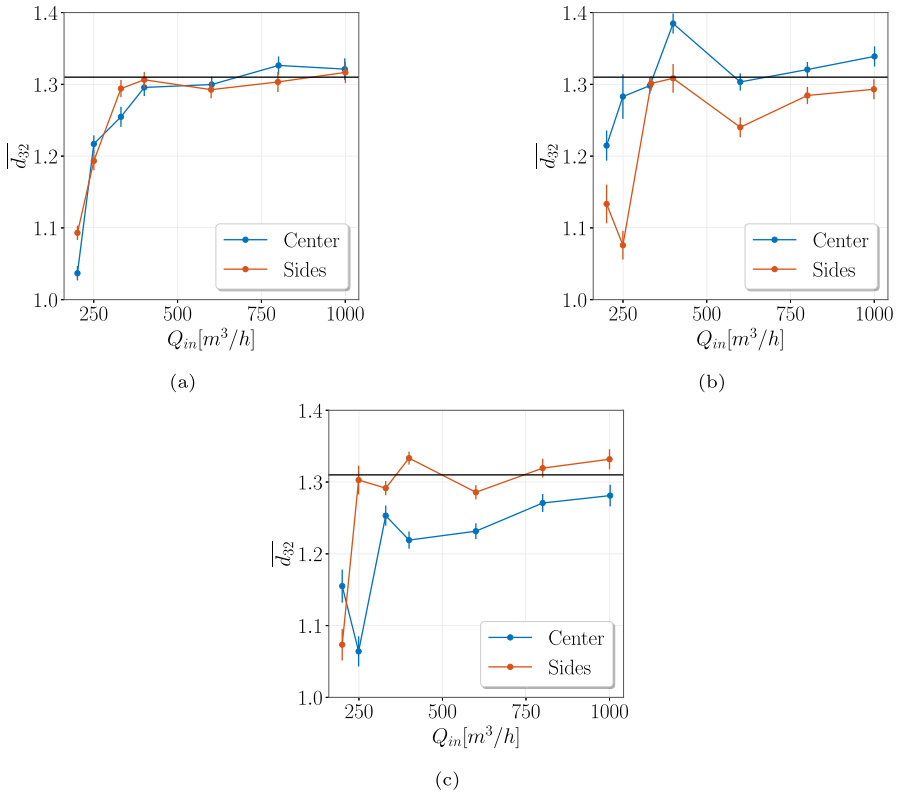

Fig. 11. Evolution of local particle segregation on top of the bed for (a) homogeneous, (b) center and (c) side aeration. The horizontal line indicates the average grain size of the whole bed.

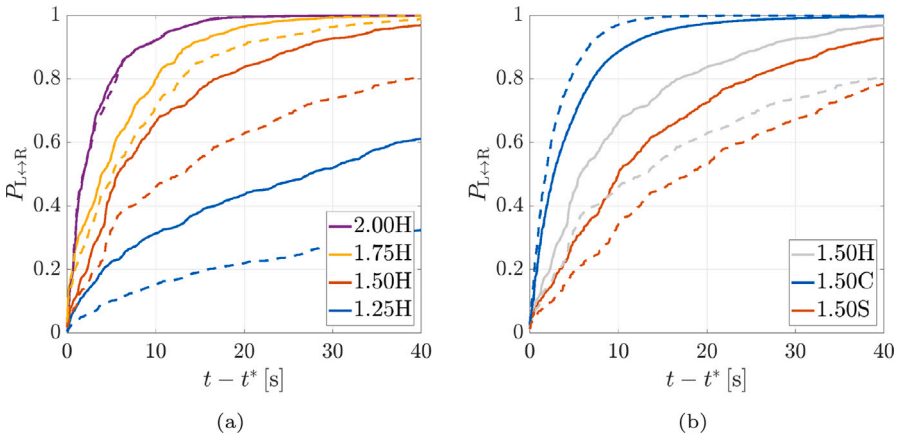

Fig. 12. Probability for a particle to change domain side at least once for (a) the total inflow and (b) the control actuation, for particles with diameter $d = 2\,\text{mm}$ and $4\,\text{mm}$ (solid and dashed lines, respectively). Note that $P_{L\leftrightarrow R}$ for case 1.50H is the same on both the left and right panels, but is repeated in the latter to aid the comparison with controlled cases.

flow rates and configurations by selectively mixing and separating a bimodal particle mixture without changing the total air inserted by the blower.

A key element of this control technique is the fact that particle segregation is a process with longer time scales than those required to change the aeration configuration, and that such a modification is at least as impactful on segregation as that of a significant increase of total flow rate. Simulations of one hypothetical scenario cycling the three aeration configurations were also carried out, confirming that segregation can be significantly reduced over longer operation time. A secondary effect of alternating aeration is to improve mixing in the bed. The control we propose could be used to clear over-wetted or overgrown particles from the distributor plate and direct them to the outlet, or to prevent excessive growth before it occurs, thus reducing the amount of shut-downs required in the process.

Due to the preliminary nature of this study, we did not include granulation in the test case, thus making it impossible to study how this control affects the entire production process. The necessity of reducing the computational costs also led to a relatively small simulation case. It is possible that this reduction of size reduced the complexity of the system thus limiting which semi-periodic patterns could occur in the three aeration regimes. Last but not least, cycling the three aeration configurations could have unwanted effects on the transport of product in the lateral direction, which was not considered here either. Therefore, it is indispensable that future studies examine the effects of our control mechanism on configurations closer to production conditions.

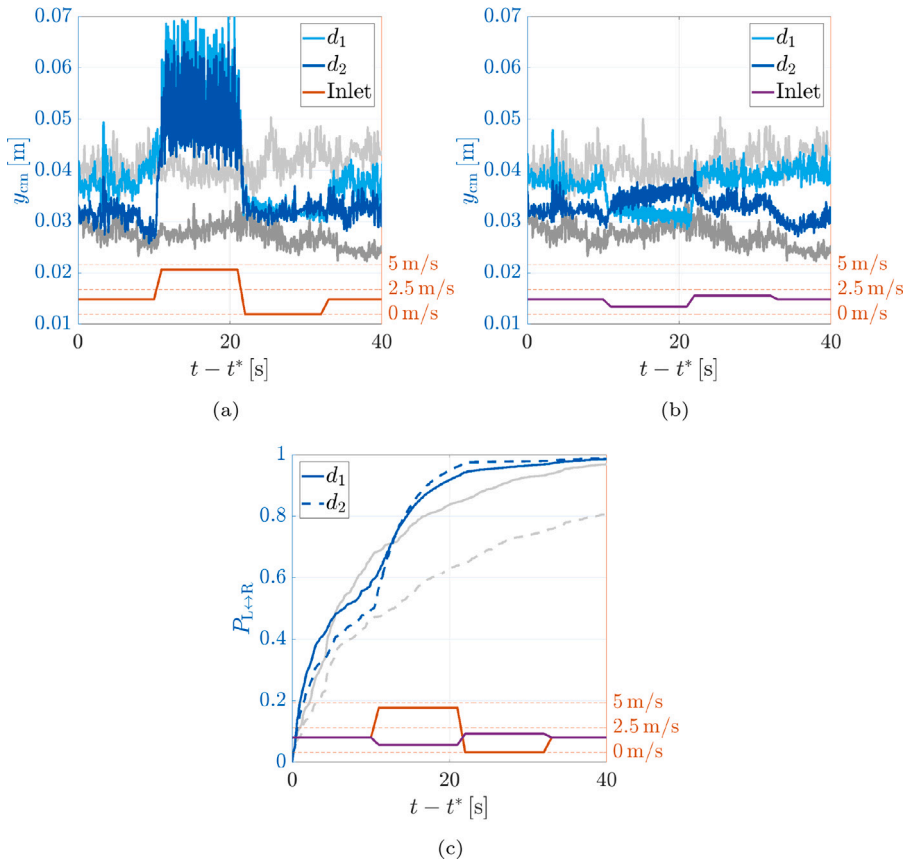

Fig. 13. Time evolution of the particle center of mass for the (a) center and (b) side regions, and (c) $P_{L\leftrightarrow R}$ are displayed for cases 1.50T and 1.50H. The latter is denoted by gray-scaled colors.

Nomenclature

Roman letter

COR	Coefficient of restitution
d_p	Particle diameter
d_1	Particle diameter (type 1)
d_2	Particle diameter (type 2)
d_{32}	Sauter diameter
$\overline{d_{32}}$	Mass-weighted Sauter diameter
$\boldsymbol{F}_{j\to i}$	Force exerted by particle j on particle i
$\boldsymbol{F}_i$	Force exerted by the fluid on particle i
$\boldsymbol{F}'_k$	Force exerted by particle k on the fluid
n_p	Number of particles
$\boldsymbol{g}$	Acceleration vector due to gravity
p	Gas pressure (Eulerian field)
q_3	Differential particle size distribution
Q_{in}	Inlet volumetric flow-rate
t	Time
t^*	Starting average time
m_i	Mass of particle i
M	Averaged solid mass in cell
$P_{L\leftrightarrow R}$	Probability of changing domain side
$\boldsymbol{u}$	Gas velocity vector (Eulerian field)
$\boldsymbol{v}_i$	Velocity vector for particle i (Lagrangian)
u	Fluid velocity in the x direction
u_p	Particle velocity in the x direction
$\overline{u_m}$	Mass-averaged velocity in the x direction
v	Fluid velocity in the y direction
v_p	Particle velocity in the y direction
$\overline{v_m}$	Mass-averaged velocity in the y direction
w	Fluid velocity in the z direction
u_{mf}	Minimum fluidization velocity
u_{S1}	Inflow velocity over left patch
u_C	Inflow velocity over central patch
u_{S2}	Inflow velocity over right patch
V	Volume of the local cell
$\boldsymbol{J}_i$	Volume of the local cell
$\boldsymbol{T}_{j\to i}$	Torque exerted by particle j on particle i
$\boldsymbol{x}_i$	Position vector for particle i (Lagrangian)
x	Horizontal coordinate parallel to produce migration
y	Vertical coordinate
y_i	Vertical coordinate of particle i
y_{cm}	Vertical coordinate of the center of mass
x	Horizontal coordinate normal to produce migration

Greek letter

Δt_{CFD}	Eulerian time step
Δt_{DEM}	Lagrangian time step
Δx	Cell size in the x direction
Δy	Cell size in the y direction
Δz	Cell size in the z direction
α	Gas volume fraction
ν	Kinematic viscosity
τ	Time, as integration variable
ρ	Gas density
ρ_s	Particle density
ρ_b	Bulk density

CRediT authorship contribution statement

A. Atxutegi: Investigation, Writing – original draft. **M. Atzori:** Investigation, Software, Writing – original draft, Writing – review & editing. **J. Bettien:** Data curation, Investigation. **T. Lichtenegger:** Conceptualization, Data curation, Project administration, Writing – original draft, Writing – review & editing. **S. Puttinger:** Data curation, Investigation, Resources, Software. **S. Pirker:** Conceptualization, Funding acquisition, Project administration, Supervision, Writing – review & editing. **S. Heinrich:** Conceptualization, Funding acquisition, Resources, Supervision, Writing – review & editing.

Declaration of competing interest

The authors declare that they have no known competing financial interests or personal relationships that could have appeared to influence the work reported in this paper.

Data availability

No data was used for the research described in the article.

Acknowledgments

M. Atzori acknowledges the financial support of the Austrian Science Fund (FWF), project number: I5180-N and A. Atxutegi is thankful for the financial support from the German Research Foundation (DFG), project number HE 4526/31-1.

References

[1] A. Bück, S. Palis, E. Tsotsas, Model-based control of particle properties in fluidised bed spray granulation, Powder Technol. 270 (2015) 575–583, http://dx.doi.org/10.1016/j.powtec.2014.07.023, 6th International Workshop on Granulation: Granulation across the length scales.

[2] E. Diez, P. Kieckhefen, K. Meyer, A. Bück, E. Tsotsas, S. Heinrich, Particle dynamics in a multi-staged fluidized bed: Particle transport behavior on micro-scale by discrete particle modelling, Adv. Powder Technol. 30 (10) (2019) 2014–2031, http://dx.doi.org/10.1016/j.apt.2019.05.025.

[3] E. Otto, R. Dürr, G. Strenzke, S. Palis, A. Bück, E. Tsotsas, A. Kienle, Kernel identification in continuous fluidized bed spray agglomeration from steady state data, Adv. Powder Technol. 32 (7) (2021) 2517–2529, http://dx.doi.org/10.1016/j.apt.2021.05.028.

[4] L. Fries, M. Dosta, S. Antonyuk, S. Heinrich, S. Palzer, Moisture distribution in fluidized beds with liquid injection, Chem. Eng. Technol. 34 (7) (2011) 1076–1084, http://dx.doi.org/10.1002/ceat.201100132.

[5] J. Zhao, W. Li, H. Qu, G. Tian, Y. Wei, Real-time monitoring and fault detection of pulsed-spray fluid-bed granulation using near-infrared spectroscopy and multivariate process trajectories, Particuology 53 (2020) 112–123, http://dx.doi.org/10.1016/j.partic.2020.02.003.

[6] R. Singh, M. Ierapetritou, R. Ramachandran, System-wide hybrid MPC–PID control of a continuous pharmaceutical tablet manufacturing process via direct compaction, Eur. J. Pharmaceut. Biopharmaceut. 85 (3, Part B) (2013) 1164–1182, http://dx.doi.org/10.1016/j.ejpb.2013.02.019.

[7] S. Palis, Control induced instabilities in fluidized bed spray granulation, J. Process Control 93 (2020) 97–104, http://dx.doi.org/10.1016/j.jprocont.2020.06.003.

[8] H. Liu, M. Li, Population balance modelling and multi-stage optimal control of a pulsed spray fluidized bed granulation, Int. J. Pharm. 468 (1) (2014) 223–233, http://dx.doi.org/10.1016/j.ijpharm.2014.04.024.

[9] A. Tamrakar, R. Ramachandran, CFD–DEM–PBM coupled model development and validation of a 3D top-spray fluidized bed wet granulation process, Comput. Chem. Eng. 125 (2019) 249–270, http://dx.doi.org/10.1016/j.compchemeng.2019.01.023.

[10] C. Goniva, C. Kloss, N.G. Deen, J.A. Kuipers, S. Pirker, Influence of rolling friction on single spout fluidized bed simulation, Particuology 10 (5) (2012) 582–591, http://dx.doi.org/10.1016/j.partic.2012.05.002.

[11] CFDEMcoupling-PFM, 2022, URL https://github.com/ParticulateFlow/CFDEMcoupling-PFM.

[12] H. Weller, G. Tabor, H. Jasak, C. Fureby, A tensorial approach to computational continuum mechanics using object-oriented techniques, Comput. phys. 12 (6) (1998) 620–631, http://dx.doi.org/10.1063/1.168744.

[13] C. Kloss, C. Goniva, A. Hager, S. Amberger, S. Pirker, Models, algorithms and validation for opensource DEM and CFD–DEM, Prog. Comput. Fluid Dyn. 12 (2–3) (2012) 140–152, http://dx.doi.org/10.1504/PCFD.2012.047457.

[14] A.P. Thompson, H.M. Aktulga, R. Berger, D.S. Bolintineanu, W.M. Brown, P.S. Crozier, P.J. in 't Veld, A. Kohlmeyer, S.G. Moore, T.D. Nguyen, R. Shan, M.J. Stevens, J. Tranchida, C. Trott, S.J. Plimpton, LAMMPS - a flexible simulation tool for particle-based materials modeling at the atomic, meso, and continuum scales, Comput. Phys. Comm. 271 (2022) 108171, http://dx.doi.org/10.1016/j.cpc.2021.108171.

[15] T.B. Anderson, R.O.Y. Jackson, A fluid mechanical description of fluidized beds, Ind. Eng. Chem. Fundam. 6 (4) (1967) 527–539.

[16] R. Beetstra, M.A. van der Hoef, J.A.M. Kuipers, Drag force of intermediate Reynolds number flow past mono- and bidisperse arrays of spheres, AIChE J. 53 (2) (2007) 489–501, http://dx.doi.org/10.1002/aic.11065.

[17] M. Tellabide, I. Estiati, A. Atxutegi, H. Altzibar, R. Aguado, M. Olazar, Fine particle flow pattern and region delimitation in fountain confined conical spouted beds, J. Ind. Eng. Chem. 95 (2021) 312–324, http://dx.doi.org/10.1016/j.jiec.2021.01.006.

[18] B. Esgandari, S. Rauchenzauner, C. Goniva, P. Kieckhefen, S. Schneiderbauer, A comprehensive comparison of two-fluid model, discrete element method and experiments for the simulation of single- and multiple-spout fluidized beds, Chem. Eng. Sci. 267 (2023) 118357, http://dx.doi.org/10.1016/j.ces.2022.118357.

[19] A. Rosato, K.J. Strandburg, F. Prinz, R.H. Swendsen, Why the Brazil nuts are on top: Size segregation of particulate matter by shaking, Phys. Rev. Lett. 58 (1987) 1038.